International Journal of Hydrogen Energy 78 (2024) 682–687

Contents lists available at ScienceDirect

International Journal of Hydrogen Energy

journal homepage: www.elsevier.com/locate/he

Oxygen flow rate measurement as a whistleblower for degradation effects in PEM water electrolysis

Markus Stähler *, Andrea Burdzik, Irene Friedrich, Andreas Everwand, Fabian Scheepers

Forschungszentrum Juelich GmbH, Institute of Energy and Climate Research, IEK-14: Electrochemical Process Engineering, 52425, Juelich, Germany

ARTICLE INFO

Handling Editor: Fanglin F. Chen

Keywords:
PEM water electrolysis
Oxygen evolution rate
Globular iridium cluster
Short circuit
Degradation

ABSTRACT

This study introduces analyzes a slow-growing degradation effect that can occur when using thin catalyst-coated membranes for PEM water electrolysis. The electric current through a test cell increased during experiments in potentiostatic operation, but the oxygen evolution rate contradicted Faraday's law. Impedance measurements below the decomposition voltage of water at the beginning and end of the experiment revealed that a new electrical phase boundary (semicircle in the Gaussian plane) arose. This allows electrons to flow across this phase boundary without triggering electrochemical reactions. SEM/EDX cross-sectional analyses show the formation of globular iridium clusters within the membrane, which grow from the anode through the membrane to the cathode. These clusters, whose formation is not yet understood, are most likely responsible for the formation of slowly-increasing short circuits between the electrodes.

1. Introduction

Polymer electrolyte membrane (PEM) water electrolysis is a technique for the electrochemical production of hydrogen. It can play an important role in building an energy supply with reduced carbon dioxide emissions [1–3]. The PEM electrolysis stacks required for this are constructed, inter alia, with catalyst-coated membranes (CCMs), which contain platinum catalysts on their cathodes, iridium oxides on their anodes, and a membrane in between. In these CCMs, hydrogen and oxygen are produced using electrical energy [2]. High conversion efficiency and a long shelf life are required to produce marketable systems [4–6]. The more stable the CCMs are, the lower the cost of producing hydrogen is [7,8].

Therefore, research groups perform long-term measurements to investigate the stability of the materials used. Degradation topics such as membrane-thinning or iridium dissolution, as well as the formation of short circuits, have already been identified and represent current research topics [9–17]. The issue of short circuits, i.e., the direct flow of electrons from one electrode through the membrane to the other, becomes more important the thinner the membranes are. This is because they are more easily damaged by mechanical stress during stack assembly or operation [6,9]. However, in terms of a fixed current density, the thinner the membrane, the lower the ohmic losses are and therefore the higher the efficiency of the CCM is [6]. It is therefore important to investigate occurrences of electrical short circuits when using thin membranes in CCMs.

If the membrane of a CCM is mechanically-damaged during potentiostatic operation, electrical contact can occur between the electrodes, and so the electrical current through the CCM increases very sharply as the cell resistance drops and the power supply strives to maintain the voltage [18]. During galvanostatic operation, however, such a short circuit becomes noticeable in the form of a sharp drop in the cell voltage [19]. To date, there has been little research into whether short circuit-like effects can occur slowly, thereby simulating an increasing improvement in the cell that does not in fact occur.

This study presents, for the first time, the results of measurements performed on laboratory cells, in which the amount of oxygen developed at the anode is measured to detect the first signs of short circuits. The oxygen balance indicates that sometimes the amount of oxygen does not change as quickly as the measured current density suggests based on Faraday's law. Electrochemical impedance spectroscopy reveals that a new phase boundary is formed in the CCM during the experimental period, across which electrons can then flow directly from one electrode to the other without becoming involved in an electrochemical reaction. SEM/EDX cross-sectional analyzes of the CCMs after the experiments indicate the heterogeneous structures of globular iridium clusters at the anode, which can grow up to the cathode and then connect both electrodes.

* Corresponding author.
E-mail address: m.staehler@fz-juelich.de (M. Stähler).

https://doi.org/10.1016/j.ijhydene.2024.06.334
Received 8 March 2024; Received in revised form 22 June 2024; Accepted 25 June 2024
Available online 29 June 2024
0360-3199/© 2024 The Authors. Published by Elsevier Ltd on behalf of Hydrogen Energy Publications LLC. This is an open access article under the CC BY license (http://creativecommons.org/licenses/by/4.0/).

2. Materials and methods

2.1. CCM preparation

Anode dispersion of iridium(IV)oxide IrO_2 (Alfa Aesar, Premion) and Nafion ionomer (Chemours, D1021), cathode dispersion of platinum (60 wt% Pt on high-surface area Ketjenblack, FC catalyst) and Nafion ionomer solution are prepared according to Stähler et al. [20,21]. These were used to fabricate catalyst-coated substrates by using slot die coating, which was described in detail in earlier publications [20,21]. Pieces of the coated substrates measuring 4.2 × 4.2 cm^2 were assembled with a Nafion 212 membrane (Chemours, thickness: 50 µm) by means of hot pressing at a pressure of 2.5 MPa and temperature of 150 °C for 3 min. After cooling down, the substrates were removed, and the catalyst loadings were determined.

2.2. Test cell assembly

The CCMs were assembled into the test cell as follows: The cathode was contacted with carbon non-woven material (H15C14, Freudenberg, thickness: 180 +/4 µm, active area: 4 × 4 cm^2). The carbon material, compressed to 100 µm thickness by using a 100 µm thick PTFE gasket, was in contact with a Pt-coated Titanium felt (Bekipor, Bekaert, thickness: 1 mm), which in turn is in contact with a single meander flow field, through which the electrode is flushed with water. The Titanium felt was sealed with a gasket of the same thickness so that it was not exposed to a compression. The cathode flow field used was gilded because of corrosion protection.

The anode of the CCM was contacted by a porous transport layer (PTL) system (Ti-felt, Bekipor, Bekaert, 0.3 mm thickness, Platinum-coated, in combination with a Iridium-coated Ti-felt, with 1.0 mm thickness) to a single meander flow field, which was platinized because of corrosion protection. The gasket thicknesses were selected according to titanium thicknesses. Eight tie rods of the test cell were then each tightened with a torque of 4 Nm.

With this cell assembly, the torque applied to the tie rods was transformed to a compression of the carbon material, set to 80 µm by the gaskets, in accordance with Stähler et al. [22]. The 1 mm-thick Titanium–PTLs were used to achieve a more homogeneous contact pressure distribution.

2.3. Characterization test rig

The schematic structure of the test rig used in this study is depicted in Fig. 1. The anode and cathode of the test cell were flushed with water (preheated to 80 °C ± 1 °C, conductivity: 0.2 µS*cm^{-1}, CR-EC-Sensors, JUMO GmbH & CO. KG). The gas from the water/gas mixture at the cell's exit was separated using a gas separator and the water flowed back into a storage container. The hydrogen was fed into the exhaust system, whereas the oxygen was diluted with an additional oxygen flow (fr $(O_2)_{in}$, 99.999%, Linde) to dilute the anode product gas to ensure a hydrogen content of a maximum of 2%, in the event of increased hydrogen permeation through the membrane. For safety reasons, this corresponds to the maximum permissible hydrogen in oxygen concentration in the test rig. The mass flow of the inlet oxygen flow was measured by using a mass flow meter (MFM series 358, Analyt MTC, accuracy: 0.002*(full scale)+0.004*(read value), range: 1l*min^{-1}). After the gas separator, the gas was cooled to condensate the water (dew point at the condenser outlet: 1 °C ± 1 °C), relative humidity and temperature were monitored by using a humidity sensor (HMT330, Vaisala). Hydrogen content was measured by means of a hydrogen sensor (FTC300, Messkonzept GmbH) and outlet oxygen was measured by using a mass flow meter of the same type as the inlet sensor. Calculating the oxygen flow difference, $fr(O_2)_{out}$ - $fr(O_2)_{in}$, allows the amount of oxygen produced to be determined. For impedance measurements, voltages were applied to the cell using an EIS meter (IM6 electrochemical workstation, Zahner), whereas a power supply (Gen 12.5–120, TDK Lambda) was employed for the constant voltage measurements.

2.4. Characterization process

After installing the test cell into the test rig and flushing the anode and cathode with water, the preheaters and test cell were heated to 80 °C for 1 h while the water was pumped in circles. To ensure that the CCM was not damaged during assembly and no short circuit occurred between the anode and cathode, constant voltage and impedance measurements were carried out after the warm-up period as follows:

In the first part of the characterization process (characterization step 1), a DC (Direct Current) voltage U_i, significantly smaller than the electrochemical decomposition voltage of water, was applied between the anode and cathode for 60 min while the DC current was measured.

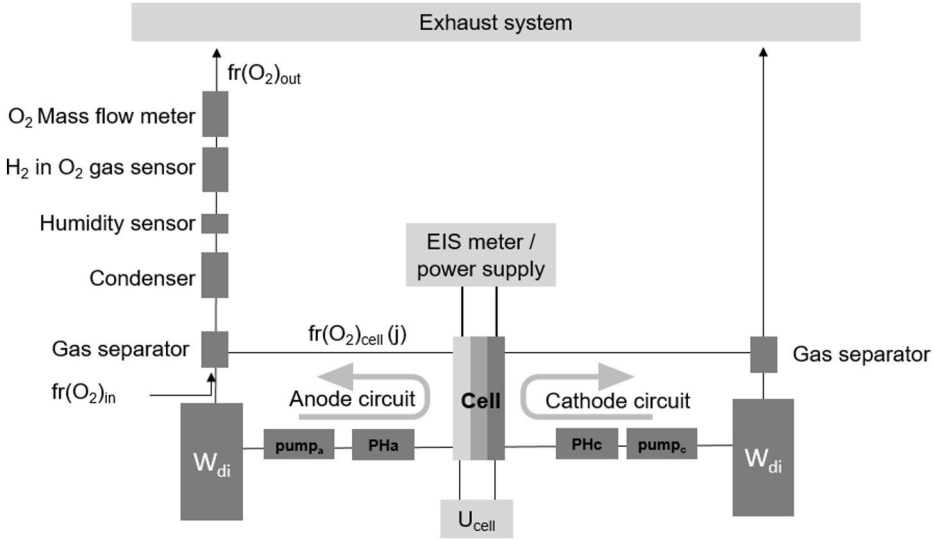

Fig. 1. Schematic representation of the test rig used. On each side, deionized water is pumped into the anode and cathode via a peristaltic pump and preheater (PH_a, PH_c). If a voltage is applied by the power supply and water in the cell is decomposed into hydrogen and oxygen, the gas separator on the cathode side feeds the hydrogen into the exhaust system. At the anode, the separated oxygen is diluted with additional oxygen and the mixture is fed into a condenser, a humidity sensor, a hydrogen sensor, and a mass flow meter for the oxygen.

This was to ensure that a steady state had been established. An EIS measurement was then carried out between 30 kHz and 10 mHz with an AC (Alternating Current) amplitude of 1 mV (approximate measurement duration: 45 min). To ensure that no drift occurred during the EIS measurement, the direct current was then measured for additional 10 min. In the end, the DC voltage and current, as well as the low frequency resistance (R_{LF}) of the impedance spectra, were used to estimate the electrical resistance between the anode and cathode. Due to possible start-up behavior of the CCM and the long duration of the measurement, the results can indicate hysteresis. To verify this, the chosen voltage was first increased and then decreased. Overall, the following DC voltages were chosen for the first part of the characterization process: $U_i = 50$ mV, 100 mV, 150 mV, 200 mV, 150 mV, 100 mV, and 50 mV. All applied voltages were less than 300 mV to ensure that no oxidation of the iridium occurred [14]. After the measurement was performed, the impedance analyzer was disconnected, and the power supply connected to the cell.

The second part of the characterization process (characterization step 2) consisted of monitoring the current density j and the flow rates fr $(O_2)_{out}$ and fr$(O_2)_{in}$ for approximately six days while the cell voltage was adjusted to a constant value of 1.65 V by the power supply. At the end of this segment, the cell voltage was set to zero and the impedance analyzer again connected to the cell.

While the first part of the characterization was intended to ensure that no damage was caused to the CCM during test cell assembly, which could lead to a short circuit, the second part, the six-day measurement, was about operating the cell under constant conditions.

After the six days in which the changed oxygen flow rate was observed, it should be clarified whether the initial state of the cell had changed, for example due to a short circuit, or whether there was a drift in the test rig during the measurement, for example due to leaks or drift of the measuring devices used.

For this reason, in a third characterization step, the impedances of the test cell were measured again at different cell voltages, as in the first characterization step. Parallel to these impedance measurements, the measured values fr$(O_2)_{in}$ and fr$(O_2)_{out}$ were recorded to ensure that the difference was zero and leakage could be excluded.

2.5. Cross-sectional analysis

The test cells were disassembled at the end of the experiments and the CCMs dried. Various samples of the CCMs were cut, embedded in resin (EpoxiFix, Struers), and polished (TegraPol-21, Struers). The cross-sectional analyses were carried out using SEM/EDX (Gemini Ultra plus, Zeiss/Ultim Max 100, Oxford).

3. Results and discussion

Several CCM samples were examined using the procedure described in section 2. Fig. 2 shows a representative progression that occurred in many samples:

The impedance investigations, as per the characterization process part 1, prove that the electrical cell resistance, measured by applying a voltage far below the electrochemical decomposition voltage of water, is at least several hundred Ωcm^2, and so the electrical current flow can be neglected (see Fig. 2B). As a result, the amount of oxygen produced during cell operation correlates with the expected value according to Faraday's law.

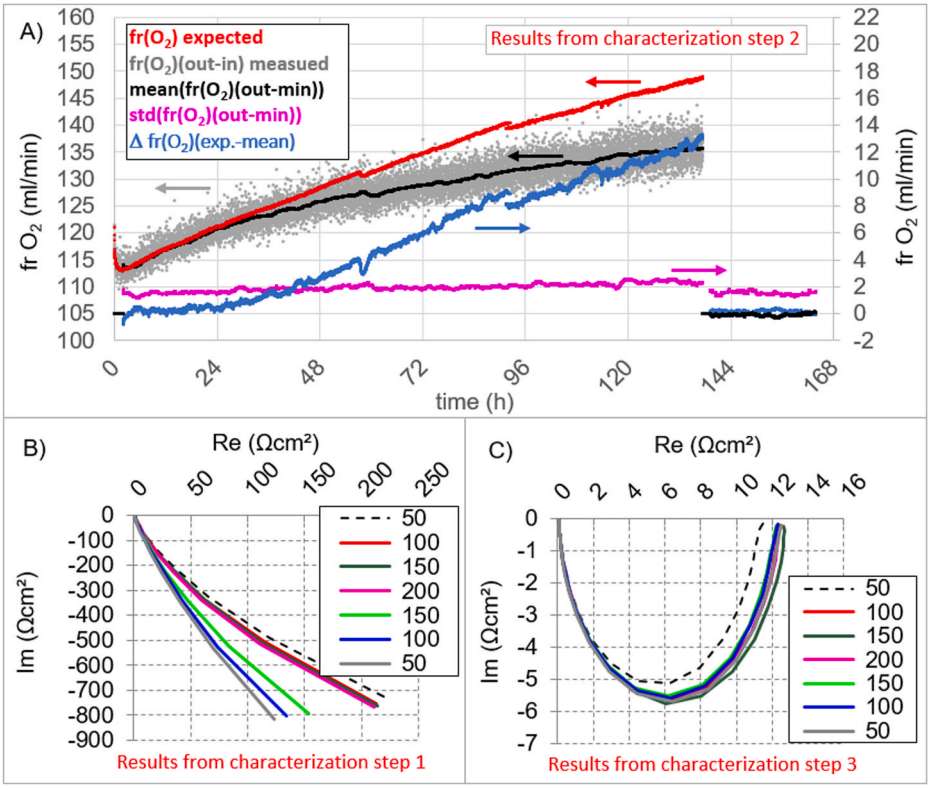

Fig. 2. A) Representation of the oxygen flow rates (fr) as a function of the measurement time (results from characterization step 2). The expected flow rate fr $(O_2)_{expected}$, calculated based on the electric current, increased more after 24 h than the measured and averaged flow rate difference between the outlet and inlet flow rates (mean(fr(O_2)(out-in))). After approximately 137 h, the power was turned off and the outlet and inlet flow rates were identical, i.e., the mean(fr(O_2)(out-in)) = 0. B) impedance values before (results from characterization step 1); and C) after the experiment for the cell voltage values between 50 mV and 200 mV (results from characterization step 3). The impedance value for low frequencies decreases from several hundred Ωcm^2 to 12 Ωcm^2, which indicates that an electrical phase boundary formed during the experiment.

$$fr(O_2)_{expected} = \frac{j \bullet A \bullet R \bullet T_n}{4 \bullet F \bullet p_n} \quad (1)$$

Equation (1): Faraday law for anode oxygen production: j-current density, A-active cell area, F-Faraday constant, p_n-standard pressure 101325 Pa, T_n-standard temperature 273.15 K, R-ideal gas constant 8.314 $Jmol^{-1}K^{-1}$,

This can be seen in Fig. 2A, where the expected oxygen flow rate fr $(O_2)_{expected}$ (red curve) according to the measured current density and Faraday's law is identical to the mean value of the difference in the outflow and inflow rate mean(fr(O_2)(out-in)) (black curve). This mean value is calculated by averaging the measured value (fr$(O_2)_{out}$ - fr$(O_2)_{in}$) over 1 h. Unfortunately, the evolution of gas in the cell and the two-phase flow of the gas–water mixture from the cell outlet to the gas separator leads to pressure drops, which result in signal scattering in the mass flow meters used. This signal scattering (shown in Fig. 2A as std(fr (O_2)(out-in)), magenta curve) is in the range of 2 $ml*min^{-1}$ and therefore in the range of measurement uncertainty due to the accuracy of the MFM sensors (see section 2.3).

The difference, Δfr(O_2)(exp.-mean), between the expected flow rate and mean flow rate (blue curve in Fig. 2A) is zero within the measurement uncertainty for the first 24 h. After this time, both values drift apart and Δfr(O_2)(exp.-mean) increases. Approximately six days later, the difference is increased to almost 13 $ml*min^{-1}$. By switching off the power supply after approximately 138 h, the electrochemical oxygen production was stopped. The data between 138 h and 163 h in Fig. 2A show that fr$(O_2)_{out}$ and fr$(O_2)_{in}$ were identical within the uncertainty and the mean(fr(O_2)(out-in)) went to zero. Therefore, no hint of a leakage or sensor drift exists.

Fig. 2C shows the impedance values, measured in characterization step 3. It can clearly be seen that an almost perfect semicircle was formed during the experiment with a low-frequency resistance R_{LF} of approximately 12 Ωcm^2. According to the theory of impedance spectroscopy [23,24], a semicircle in the Gaussian plane can be interpreted as an electrical phase boundary where charge flows through a resistor R (circular diameter) to which a capacitance C is connected in parallel. The negligible dependency of the semicircular diameter on the applied DC voltage in the range between 50 mV and 200 mV suggests that the underlying process is not an electrochemical one. With the frequency of the impedance with the lowest imaginary part ($f_m = 0.7\ s^{-1}$, Fig. 2C), it is possible to estimate the capacity C by using the following formula, taken from Ref. [19]:

$$Z_{R\|C} = \frac{R - i \bullet \omega \bullet R^2 \bullet C}{1 + \omega^2 \bullet R^2 \bullet C^2};\ \left.\frac{\partial imag(Z_{R\|C})}{\partial \omega}\right|_{f_m} = 0 \rightarrow C = \frac{1}{2 \bullet \pi \bullet f_m \bullet R} \quad (2)$$

Equation (2): Impedance for a parallel RC circuit, which can be used to describe electrically a phase boundary. The determination of the frequency used for the lowest imaginary value of Z allows to determine the capacity value.

With $R = R_{LF} = 12\ \Omega cm^2$ and an active area of 16 cm^2 this results in a capacity value of approximately 0.3 F. Due to this high capacitance value, it is somewhat unlikely that a technical failure, e.g., a metal fiber that pierced the membrane during operation, could be the physical reason for the formation of the electrical phase boundary detected.

The reduction in the expected oxygen evolution rate and the formation of a new electrical phase boundary could be observed in many CCMs after the experiment. Fig. 3A shows the Δfr(O_2)(exp.-mean) values after approximately six days for CCM samples with different catalyst loadings. Although the values were subject to a measurement uncertainty of approximately 2 $ml*min^{-1}$, the results were included to make it clear that thus far, no correlation has been observed between the Δfr(O_2)(exp.-mean) values and catalyst loadings (Fig. 3A).

The deviations between fr$(O_2)_{expected}$ and Δfr(O_2)(exp.-mean) must depend on this electrical phase boundary, because the current flowing through it is not involved in an oxygen evolution reaction. If a parallel $R_{LF}|C$ circuit is used to describe this phase boundary, an anti-proportional correlation between R_{LF} and the short-circuit current density j_{sc} is to be expected when a constant voltage U is applied. Consequently, the correlation between Δfr(O_2)(exp.-mean) and R_{LF} must show the same anti-proportional course (see Fig. 3B).

To find evidence for the formation of new electrical phase boundaries between the electrodes, numerous cross-sectional analyses were carried out on the examined CCMs using SEM/EDX. The results are presented in Fig. 4.

The cross-section of the CCMs shows a heterogeneous formation of globular clusters near the anode (Fig. 4A, lower area). Lettenmeier et al. [25] reported a similar formation of an iridium band close to the IrO_2 anode of a Nafion 115 CCM after a 750 h test, but they did not elaborate on this observation. Padgett et al. [26] also revealed an iridium band close to the IrO_2 anode of a Nafion 115 CCM after a 500 h test. Grigoriev et al. [27] presented results from an analysis of an element distribution in a cross section of a CCM with a Nafion 117 membrane. They found among other elements agglomerates of iridium in the anode, membrane and cathode, but without but without any indication of a connection

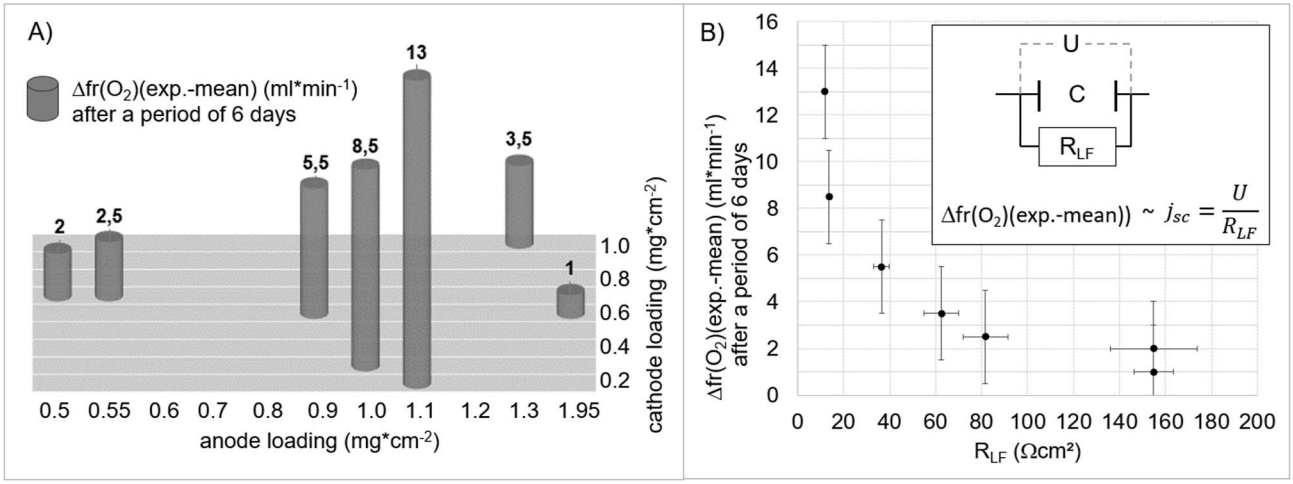

Fig. 3. Δfr(O_2)(exp.-mean)-values (measurement uncertainty of ± 2 $ml*min^{-1}$). A) As a result of seven experiments with different CCMs and catalyst loadings at the cathode and anode – a dependence on the catalyst loading is not visible; B) as a function of the measured low-frequency impedance values (R_{LF}) of seven experiments. The inlet picture shows the relationship between the short circuit current density j_{sc} and the applied voltage U. When the short circuit resistance R_{LF} is reduced, j_{sc} correlates anti-proportionally to R_{LF}.

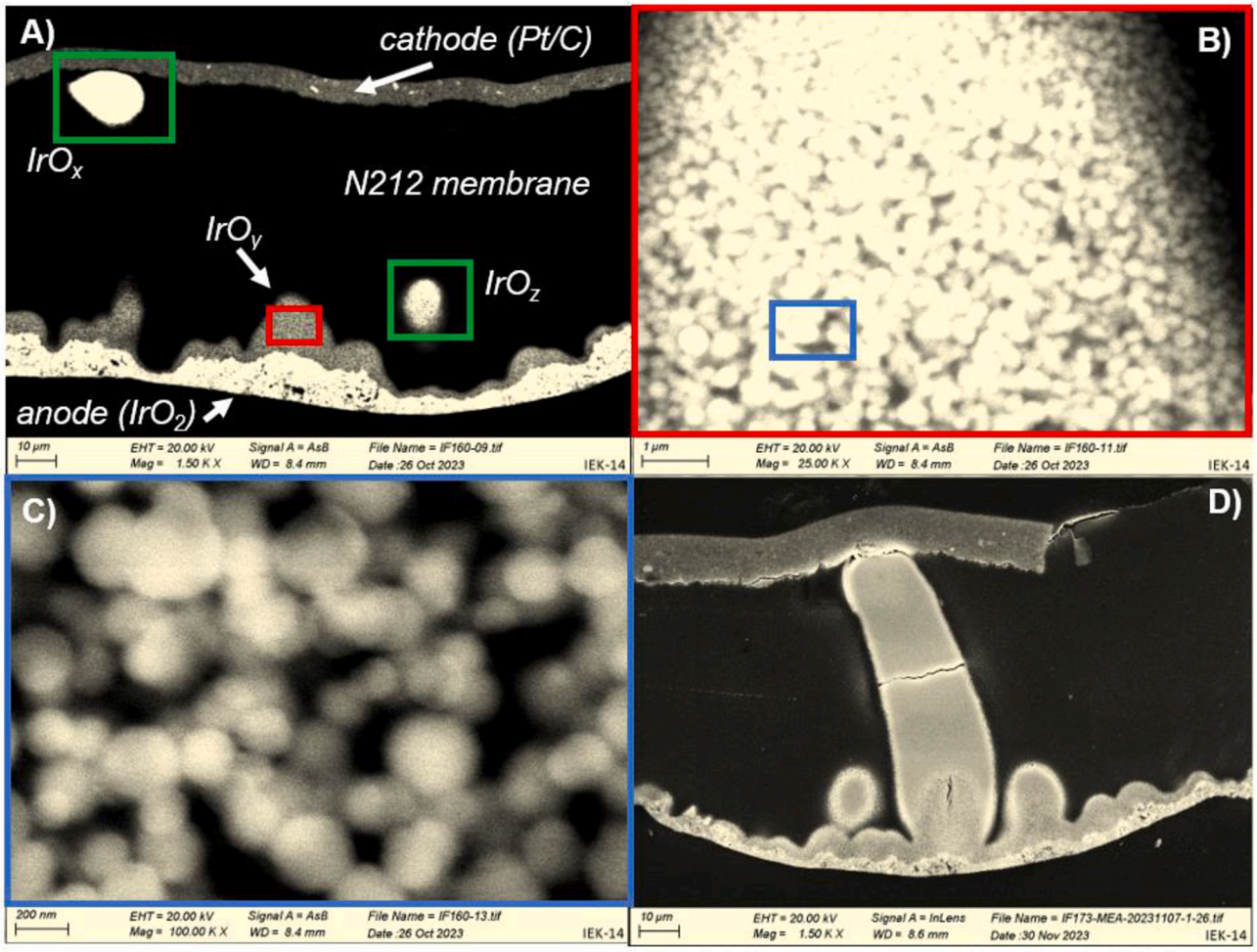

Fig. 4. A) Cross-section of a CCM after the long-term test. EDX measurements prove that the areas marked in red and green contain mostly iridium. It is unknown whether the iridium/oxide ratios are identical. B) Enlargement of the red marked area of A); together with a further magnification of the area marked in blue, the globular iridium cluster becomes clear in C); D) this globular iridium cluster can grow from the anode to the cathode and form a connection. Due to possible oblique growth, the green-marked areas in A) are interpreted as obliquely-grown structures that were cut during sample preparation. (For interpretation of the references to colour in this figure legend, the reader is referred to the Web version of this article.)

between the electrodes. Unfortunately, none of the authors reported a short-circuit analysis of the CCMs or presented the measured amount of oxygen evolved, and so a direct comparison with the data discussed in the present study is unfortunately not possible.

Fig. 4B shows an enlargement of the red marked area of Fig. 4A, whereas Fig. 4C shows an enlargement of the blue marking in Fig. 4B. The cluster structure is clearly visible and EDX measurements prove that these particles, which are a few hundred nanometers in size, have a high iridium content.

The bright areas in Fig. 4A (marked in green) are mostly comprised of iridium. Fig. 4D depicts a cluster structure consisting mostly of iridium that connects both electrodes. Apparently, these clusters can grow obliquely through the membrane, such that sometimes only parts of them can be seen, depending on how the CCM is cut during sample preparation. This is the most likely explanation for the areas highlighted in green in Fig. 4A.

These globular iridium clusters can account for the discovered new electrical phase boundary between the electrodes: a loose contact between many small metal-containing particles, which can form a connection between the electrodes and, due to their size of a few hundred nanometers, a very large area is created between the particles.

Thus far, the cause of the formation of these clusters is unclear. It is also unclear how much current flows through these structures. Based on the measured impedance value $R_{LF} = 12\ \Omega cm^2$, a short circuit current density of 0.138 Acm^{-2} can be expected at 1.65 V. According to Equation (1), a missing oxygen flow rate of approximately 7.7 $ml*min^{-1}$ can be explained by this measured electrical phase boundary. This corresponds to only approximately about 70 % of the measured $\Delta fr(O_2)$ value. Therefore, further effects are expected, and more in-depth studies are required to understand the formation of the globular iridium cluster and the correlation to the measured electrical phase boundary.

The reason for publishing this data from the ongoing study is to make the PEM water electrolysis community aware of this short-circuiting problem and thus encourage others to participate in developing countermeasures against this phenomenon.

4. Conclusions

The results of electrochemical measurements in which CCMs for PEM water electrolysis were operated constantly at 1.65 V for about six days show that during this time, the oxygen flow rate did not correspond to the gas amount calculated using Faraday's law. A pre- and post-test impedance investigation revealed that a new electrical phase boundary was formed during the test, allowing a direct electrical current flow from the anode to the cathode without an electrochemical reaction. This formation of an electrical phase boundary was different for several CCMs examined with different catalyst loadings. A relationship between the loading and this formation could not be observed. SEM/EDX studies

indicated the formation of globular iridium clusters within the membrane, which can grow from the anode to the cathode. It is likely that these clusters are the physical explanation for the new electrical phase boundary detected using impedance spectroscopy.

Further investigations of this cluster formation should be carried out in future work. Perhaps more attention should be paid to the iridium accumulations in the membrane phase already described in previous publications, as these could lead to short circuits in the CCMs during operation. The impedance investigations shown below the decomposition voltage of water before and after long-term tests can be used to detect such short circuits, whereas online oxygen flow rate measurement proved a suitable method for detecting their formation during the experiments.

Funding

Funded by the Deutsche Forschungsgemeinschaft (DFG, German Research Foundation) – 491111487.

CRediT authorship contribution statement

Markus Stähler: Formal analysis, Investigation, Methodology, Supervision, Validation, Visualization, Writing – original draft, Writing – review & editing. **Andrea Burdzik:** Formal analysis, Investigation, Methodology, Supervision, Validation, Writing – original draft. **Irene Friedrich:** Investigation, Methodology. **Andreas Everwand:** Investigation, Methodology. **Fabian Scheepers:** Formal analysis, Writing – original draft.

Declaration of competing interest

The authors declare that they have no known competing financial interests or personal relationships that could have appeared to influence the work reported in this paper.

Acknowledgements

We gratefully acknowledge Thomas Pütz and Hakim Kerroumi for their extensive and professional support in developing the test rig components. Furthermore, we would like to thank Christopher Wood for proofreading the manuscript.

References

[1] Ayers K, Danilovic N, Ouimet R, Carmo M, Pivovar B, Bornstein M. Perspectives on low-temperature electrolysis and potential for renewable hydrogen at scale. Annu Rev Chem Biomol Eng 2019;10:219–39.
[2] Carmo M, Fritz DL, Mergel J, Stolten D. A comprehensive review on PEM water electrolysis. Int J Hydrogen Energy 2013;38:4901–34.
[3] Shiva Kumar S, Himabindu V. Hydrogen production by PEM water electrolysis – a review. Materials Science for Energy Technologies 2019;2:442–54.
[4] Minke C, Suermann M, Bensmann B, Hanke-Rauschenbach R. Is iridium demand a potential bottleneck in the realization of large-scale PEM water electrolysis? Int J Hydrogen Energy 2021;46:23581–90.
[5] Taie Z, Peng X, Kulkarni D, Zenyuk IV, Weber AZ, Hagen C, et al. Pathway to complete energy sector decarbonization with available iridium resources using ultralow loaded water electrolyzers. ACS Appl Mater Interfaces 2020;12:52701–12.
[6] Babic U, Suermann M, Büchi FN, Gubler L, Schmidt TJ. Critical review—identifying critical gaps for polymer electrolyte water electrolysis development. J Electrochem Soc 2017;164:F387.
[7] Mayyas AT, Ruth MF, Pivovar BS, Bender G, Wipke KB. Manufacturing cost analysis for proton exchange membrane water electrolyzers. United States2019.
[8] Proost J. Critical assessment of the production scale required for fossil parity of green electrolytic hydrogen. Int J Hydrogen Energy 2020;45:17067–75.
[9] Grigoriev SA, Dzhus KA, Bessarabov DG, Millet P. Failure of PEM water electrolysis cells: case study involving anode dissolution and membrane thinning. Int J Hydrogen Energy 2014;39:20440–6.
[10] Millet P, Ranjbari A, de Guglielmo F, Grigoriev SA, Auprêtre F. Cell failure mechanisms in PEM water electrolyzers. Int J Hydrogen Energy 2012;37:17478–87.
[11] De Moor G, Charvin N, Bas C, Caque N, Rossinot E, Flandin L. In situ quantification of electronic short circuits in PEM fuel cell stacks. IEEE Trans Ind Electron 2015;62:1.
[12] Badwal SPS, Giddey S, Ciacchi FT. Hydrogen and oxygen generation with polymer electrolyte membrane (PEM)-based electrolytic technology. Ionics 2006;12:7–14.
[13] Cherevko S, Geiger S, Kasian O, Mingers A, Mayrhofer KJJ. Oxygen evolution activity and stability of iridium in acidic media. Part 2. - electrochemically grown hydrous iridium oxide. J Electroanal Chem 2016;774:102–10.
[14] Cherevko S, Geiger S, Kasian O, Mingers A, Mayrhofer KJJ. Oxygen evolution activity and stability of iridium in acidic media. Part 1. - metallic iridium. J Electroanal Chem 2016;773:69–78.
[15] Geiger S, Kasian O, Shrestha BR, Mingers AM, Mayrhofer KJJ, Cherevko S. Activity and stability of electrochemically and thermally treated iridium for the oxygen evolution reaction. J Electrochem Soc 2016;163:F3132–8.
[16] Milosevic M, Böhm T, Körner A, Bierling M, Winkelmann L, Ehelebe K, et al. In search of lost iridium: quantification of anode catalyst layer dissolution in proton exchange membrane water electrolyzers. ACS Energy Lett 2023;8:2682–8.
[17] Wallnöfer-Ogris E, Grimmer I, Ranz M, Höglinger M, Kartusch S, Rauh J, et al. A review on understanding and identifying degradation mechanisms in PEM water electrolysis cells: insights for stack application, development, and research. Int J Hydrogen Energy 2024;65:381–97.
[18] Grumm F, Schumann M, Cosse C, Plenz M, Lücken A, Schulz D. Short circuit characteristics of PEM fuel cells for grid integration applications. Electronics2020.
[19] Abdel-Motagali A, Al Bacha SMA, El Rouby W, Bigarré J, Millet P. Evaluating the performance of hybrid proton exchange membrane for PEM water electrolysis. Int J Hydrogen Energy 2024;49:87–102.
[20] Stähler A, Stähler M, Scheepers F, Lehnert W, Carmo M. Scalable implementation of recombination catalyst layers to mitigate gas crossover in PEM water electrolyzers. J Electrochem Soc 2022;169:034522.
[21] Stähler M, Stähler A, Scheepers F, Carmo M, Stolten D. A completely slot die coated membrane electrode assembly. Int J Hydrogen Energy 2019;44:7053–8.
[22] Stähler M, Stähler A, Scheepers F, Carmo M, Lehnert W, Stolten D. Impact of porous transport layer compression on hydrogen permeation in PEM water electrolysis. Int J Hydrogen Energy 2020;45:4008–14.
[23] Lazanas AC, Prodromidis MI. Electrochemical impedance Spectroscopy—A tutorial. ACS Measurement Science Au 2023;3:162–93.
[24] Macdonald JR, Johnson WB. Fundamentals of impedance spectroscopy. Impedance Spectroscopy2005. p. 1-26.
[25] Lettenmeier P, Wang R, Abouatallah R, Helmly S, Morawietz T, Hiesgen R, et al. Durable membrane electrode assemblies for proton exchange membrane electrolyzer systems operating at high current densities. Electrochim Acta 2016;210:502–11.
[26] Padgett E, Bender G, Haug A, Lewinski K, Sun F, Yu H, et al. Catalyst layer resistance and utilization in PEM electrolysis. J Electrochem Soc 2023;170:084512.
[27] Grigoriev SA, Bessarabov DG, Fateev VN. Degradation mechanisms of MEA characteristics during water electrolysis in solid polymer electrolyte cells. Russ J Electrochem 2017;53:318–23.